

and lead citrate for transmission electron microscopy using a Philips 208S.

30. For supplemental data, see *Science Online* ([www.sciencemag.org/cgi/content/full/293/5534/1487/DC1](http://www.sciencemag.org/cgi/content/full/293/5534/1487/DC1)).

31. J. Mikol, S. Brion, L. Guicharnaud, O. Waks, *Acta Neuropathol.* **49**, 57 (1980).

32. Studies of the JNPL3 mice have indicated that there are sex differences in the development of NFT pathology. Female mice have higher tau expression in the central nervous system relative to males (in situ hybridization, Northern, and Western analysis) and develop tau pathology and motor disturbance at an earlier age. Similar higher levels of tau expression in female mice have also been observed in a second transgenic mouse line expressing the longest 4R tau isoform with the P301L mutation.

33. M. J. Callahan *et al.*, *Am. J. Pathol.* **158**, 1173 (2001).

34. A. F. Jorm, A. E. Korten, A. S. Henderson, *Acta Psychiatr. Scand.* **76**, 465 (1987).

35. W. A. Rocca *et al.*, *Ann. Neurol.* **30**, 381 (1991).

36. C. H. Kawas, R. Katzman, in *Alzheimer Disease*, R. D. Terry, R. Katzman, K. L. Bick, S. Sisodia, Eds. (Lippincott Williams & Wilkins, Philadelphia, ed. 2, 1999), pp. 95–116.

37. For A $\beta$  measurements, one hemisphere was dounce-homogenized in 70% formic acid and centrifuged at 100,000g for 1 hour; the resulting supernatant was neutralized by a 1:20 dilution in 1 M tris base followed by dilution in buffer EC (0.02 M NaH<sub>2</sub>PO<sub>4</sub>, 0.002 M EDTA, 0.4 M NaCl, 0.2% BSA, 0.05% CHAPS, 0.04% BlockAce, 0.05% NaN<sub>3</sub>, pH 7.0). A $\beta$  values were determined by sandwich enzyme-linked immunosorbent assay (ELISA) using the BAN50/BA27 and BAN50/BC05 ELISA systems for A $\beta$ 40 and A $\beta$ 42, respectively. The values presented were calculated by determining the amount of A $\beta$  detected relative to synthetic human A $\beta$ 1–40 and A $\beta$ 1–42 and converting to pmol per gram of wet weight of brain.

38. S. A. Gravina *et al.*, *J. Biol. Chem.* **270**, 7013 (1995).

39. S. J. Haugabook *et al.*, *FASEB J.* **15**, 16 (2001).

40. For total soluble tau Western blots, mouse brains were harvested and snap-frozen; immunoblotting was performed by homogenizing half of a mouse brain in buffer containing protease inhibitor (1 mM phenylmethylsulfonyl fluoride, 20  $\mu$ M aprotinin, 10  $\mu$ M leupeptin, and 1 mM EGTA) and phosphatase inhibitor (5 mM sodium pyrophosphate, 30 mM  $\beta$ -glycerophosphate, and 30 mM sodium fluoride). Homogenates were dissolved in sample buffer and run on a 10% SDS–polyacrylamide gel electrophoresis (PAGE) gel, transferred to nitrocellulose, and stained with a human tau-specific antibody, E1, and an antibody that recognizes mouse and human tau (WKS45). Equivalent sample loading was determined by protein assay and confirmed by probing the tau blots with an antibody to  $\beta$ -tubulin (Sigma). The antibody, E1, was raised to amino acid residues 19 to 33 of human tau. WKS45 is a polyclonal antibody that recognizes mouse and human tau (amino acids 258 to 266). Quantitation of Western blots was performed by image analysis using MCID software (Research System Inc.). The ratio of tau to tubulin in different samples was compared.

41. For Northern analysis, total RNA was extracted from crushed whole mouse brains using Trizol (Life Technologies); RNA (15  $\mu$ g) was electrophoresed on a denaturing gel, transferred overnight onto a nylon membrane (Hybond-N<sup>+</sup>, Amersham Life Science), and cross-linked. An oligomer designed to exon 11 of human/mouse tau (5'-AGATTTTACTTCCACCTGGCCACCTCTG-3') was used to assess transgenic mRNA levels. Probes were 3' end-labeled with [ $\alpha$ -<sup>32</sup>P]deoxyadenosine triphosphate. The membrane was hybridized in buffer [containing 4 $\times$  SSC, 1 $\times$  Denhardt's solution, 50% (w/v) deionized formamide, 10% (w/v) dextran sulfate, and herring sperm DNA (200 mg/ $\mu$ l)] with the labeled probe overnight at 42°C. The membrane was washed stringently (1 $\times$  SSC/0.1% SDS at 55°C) and exposed to Biomax maximum-sensitivity film (Kodak) at –80°C and Amersham Phosphor Imaging Screens for 1 to 2 days. Band quantification was performed using a Storm Phosphor scanner and ImageQuant software (Molecular Dynamics). Membranes were stripped and reprobed with a <sup>32</sup>P-labeled histone cDNA probe to assess loading.

42. For analysis of sarkosyl-insoluble tau, brain tissue (sectioned into cortex-limbic and subcortical–basal ganglia–cerebellum fractions) was homogenized in tris-buffered saline (TBS); a small sample was removed for the analysis of total tau, and the remainder was centrifuged at 100,000g for 1 hour at 4°C. The pellet was homogenized in 0.8 M NaCl and 10% sucrose in TBS. After centrifugation at 150,000g for 15 min, the supernatant was brought to 1% sarkosyl and incubated at 37°C for 1 hour. The mixture was then centrifuged at 150,000g for 30 min and the precipitate was collected as the sarkosyl-insoluble fraction. Equal amounts (v/w) of insoluble tau preparations were analyzed by SDS-PAGE and Western blotting using an antibody specific to human tau (E1, amino acids 19 to 33) and one that recognizes both human and mouse tau (WKS45, amino acids 258 to 266). Hyperphosphorylated tau was detected with PHF-1 (phospho-396/404).

43. S. G. Greenberg, P. Davies, *Proc. Natl. Acad. Sci. U.S.A.* **87**, 5827 (1990).

44. D. W. Dickson *et al.*, *Acta Neuropathol.* **85**, 463 (1993).

45. I. Vincent, J. H. Zheng, D. W. Dickson, Y. Kress, P. Davies, *Neurobiol. Aging* **19**, 287 (1998).

46. J. Hardy, K. Duff, K. Gwinn-Hardy, J. Perez-Tur, M. Hutton, *Nature Neurosci.* **1**, 355 (1998).

47. J. Götz, F. Chen, J. van Dorpe, R. M. Nitsch, *Science* **293**, 1491 (2001).

48. We thank P. Davies (Albert Einstein College of Medicine) for antibodies, V. Philips and L. Rousseau for histopathology, and D. Forste, E. Kirkham, C. Ortega, and F. Conkle for mouse maintenance. Supported by the National Institute on Aging (PO1 grant to D.W.D., S.-H.Y., J.H., M.H.), National Institute of Neurological Diseases and Stroke (M.H.), Mayo Foundation, Smith Scholar Program (J.L., C.E.), John Douglas French Alzheimer's Foundation (J.L.), MetLife Foundation (D.W.D., M.H.), and Mayo Clinic Alzheimer's Disease Research Center (E.M.).

11 December 2000; accepted 14 June 2001

## Formation of Neurofibrillary Tangles in P301L Tau Transgenic Mice Induced by A $\beta$ 42 Fibrils

J. Götz,<sup>1\*</sup>† F. Chen,<sup>1\*</sup> J. van Dorpe,<sup>2</sup> R. M. Nitsch<sup>1‡</sup>

$\beta$ -Amyloid plaques and neurofibrillary tangles (NFTs) are the defining neuropathological hallmarks of Alzheimer's disease, but their pathophysiological relation is unclear. Injection of  $\beta$ -amyloid A $\beta$ <sub>42</sub> fibrils into the brains of P301L mutant tau transgenic mice caused fivefold increases in the numbers of NFTs in cell bodies within the amygdala from where neurons project to the injection sites. Gallyas silver impregnation identified NFTs that contained tau phosphorylated at serine 212/threonine 214 and serine 422. NFTs were composed of twisted filaments and occurred in 6-month-old mice as early as 18 days after A $\beta$ <sub>42</sub> injections. Our data support the hypothesis that A $\beta$ <sub>42</sub> fibrils can accelerate NFT formation in vivo.

Transgenic mice that express P301L mutant human tau form abnormal tau-containing filaments in brains (1, 2). These filaments have striking similarities with the NFTs of several human neurodegenerative diseases, including Alzheimer's disease (AD) and frontotemporal dementia with parkinsonism linked to chromosome 17 (FTDP-17), but their numbers are considerably lower than these commonly found in human disease (3). To determine whether  $\beta$ -amyloid can accelerate NFT formation, we injected synthetic A $\beta$ <sub>42</sub> fibrils into the somato-

sensory cortex and the hippocampus of 5- to 6-month-old P301L tau transgenic mice (4) and nontransgenic littermates (5–7). For the control peptide, we used the reversed sequence, A $\beta$ <sub>42-1</sub>, derived from the identical source (6). A $\beta$ <sub>42</sub> fibrils were generated by incubation at 37°C with shaking and were confirmed by electron microscopy (Fig. 1, A and B) (5, 6). A $\beta$ <sub>42</sub> fibrils were stable in vivo in both P301L transgenic and wild-type control mice and were readily detectable at least until 45 days after the injections (Fig. 1C). As expected, brain amyloid deposits were accompanied by reactive astrogliosis at both the injection sites (Fig. 1D) and the amygdala (Fig. 1E) (8); these were seen in both A $\beta$ <sub>42</sub>- and in control-injected transgenic mice and persisted for at least 45 days after injection. This reaction may be related to the fact that neurons in the amygdala project to the injection sites, as shown by retrograde transport of Texas red–conjugated dextran from the injection site in the somatosensory cortex to cell bodies in the amygdala (Fig. 1F) (8).

Eighteen days after the injections of A $\beta$ <sub>42</sub>, Gallyas silver impregnation (9) re-

<sup>1</sup>Division of Psychiatry Research, University of Zürich, August Forel Strasse 1, 8008 Zürich, Switzerland.

<sup>2</sup>Experimental Genetics Group, Center for Human Genetics, K. U. Leuven, Campus Gasthuisberg, Leuven, Belgium.

\*These authors contributed equally to this work.  
 †To whom correspondence should be addressed at the Division of Psychiatry Research, University of Zürich, August Forel Strasse 1, 8008 Zürich, Switzerland. E-mail: goetz@bli.unizh.ch  
 ‡To whom correspondence should be addressed at the Division of Psychiatry Research, University of Zürich, August Forel Strasse 1, 8008 Zürich, Switzerland. E-mail: nitsch@bli.unizh.ch

## REPORTS

vealed numerous NFTs (Fig. 2, A to E), along with neuropil threads and degenerating neurites (Fig. 2C) in the amygdala of P301L, but not wild-type, mice. Occasional NFTs were also present in the parietal cortex (Fig. 2D). The NFTs in mice (Fig. 2E) were very similar to those in AD brains stained in parallel by the same protocol (Fig. 2F). Moreover, the neuropil threads were similar to those known in AD (10–12). A subset of Gallyas-positive NFTs in

the mice was also stained with thioflavin-S, consistent with the histopathology of AD (Fig. 2G). Immunoelectron microscopy identified many AT8-positive tau filaments in somatodendritic localizations of neurons within the basolateral amygdala of  $A\beta_{42}$ -injected P301L mice (13) (Fig. 2, H to J). The filaments had a width of 20 to 25 nm and a periodicity of 90 nm and are best described as twisted ribbons. In human carriers, the P301L mutation causes predomi-

nant expression of four repeat (4R) isoforms, with a small amount of wild-type 3R isoforms, resulting in 15-nm-wide twisted filaments with a periodicity of greater than 130 nm (14). Because mice endogenously express only 4R tau isoforms, and the transgene was designed to express 4R human P301L tau, the filaments observed here contained no 3R tau. Importantly, the human intronic FTDP-17 mutations that reduce the formation of 3R tau also cause twist-

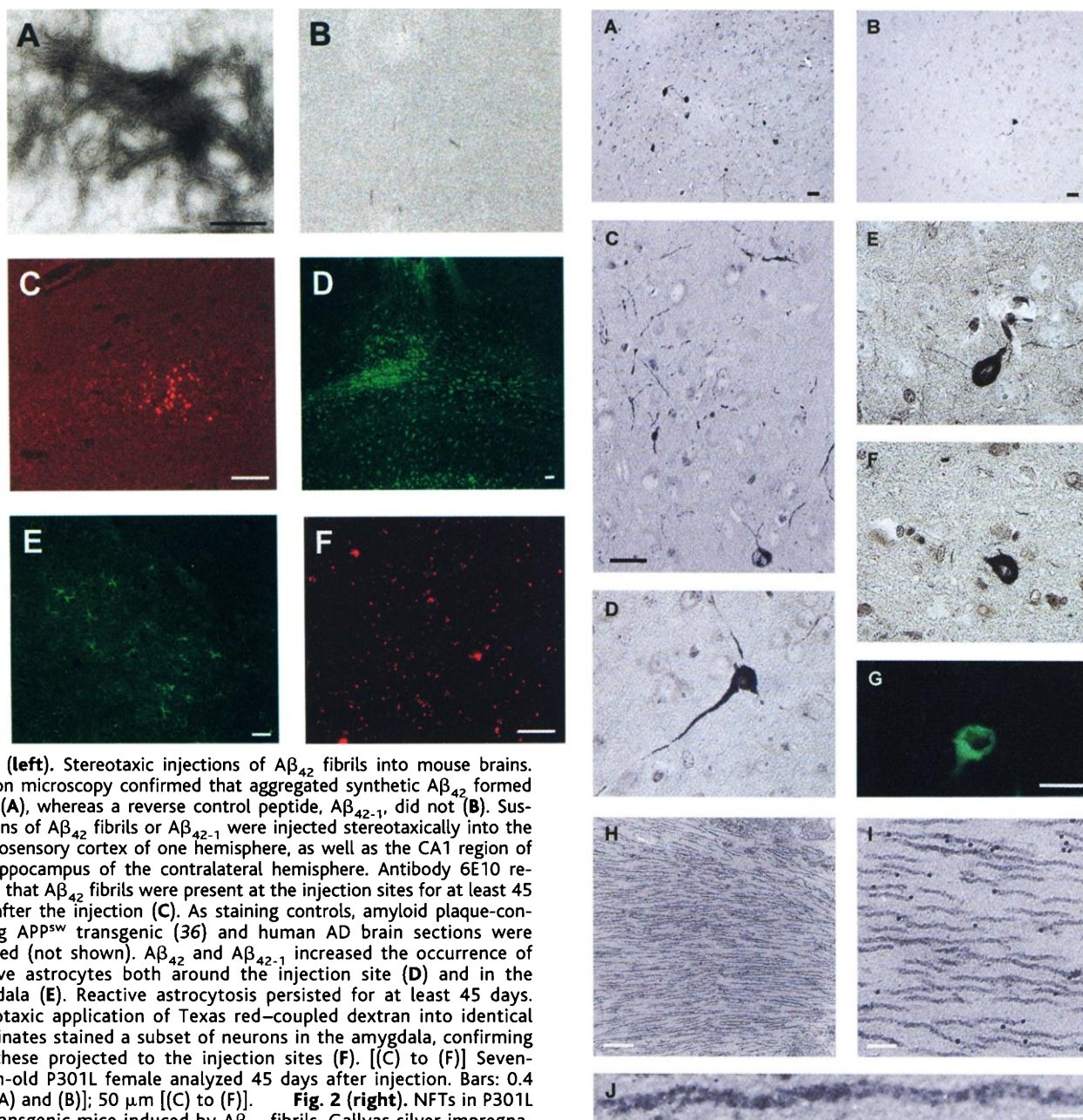


**Fig. 1 (left).** Stereotaxic injections of  $A\beta_{42}$  fibrils into mouse brains. Electron microscopy confirmed that aggregated synthetic  $A\beta_{42}$  formed fibrils (A), whereas a reverse control peptide,  $A\beta_{42-1}$ , did not (B). Suspensions of  $A\beta_{42}$  fibrils or  $A\beta_{42-1}$  were injected stereotaxically into the somatosensory cortex of one hemisphere, as well as the CA1 region of the hippocampus of the contralateral hemisphere. Antibody 6E10 revealed that  $A\beta_{42}$  fibrils were present at the injection sites for at least 45 days after the injection (C). As staining controls, amyloid plaque-containing APP<sup>sw</sup> transgenic (36) and human AD brain sections were included (not shown).  $A\beta_{42}$  and  $A\beta_{42-1}$  increased the occurrence of reactive astrocytes both around the injection site (D) and in the amygdala (E). Reactive astrogliosis persisted for at least 45 days. Stereotaxic application of Texas red-coupled dextran into identical coordinates stained a subset of neurons in the amygdala, confirming that these projected to the injection sites (F). **Fig. 2 (right).** NFTs in P301L tau transgenic mice induced by  $A\beta_{42}$  fibrils. Gallyas silver impregnations of NFTs in the amygdala of  $A\beta_{42}$ - (A) and  $A\beta_{42-1}$ -injected (B) P301L tau transgenic mice.  $A\beta_{42}$  fibrils induced the Gallyas-positive formation of numerous NFTs and neuropil threads in the amygdala and, occasionally, the cortex as early as 18 days after the injection (C to E). NFTs in mice were very similar to those found in brains obtained from AD patients; these slides were stained in parallel by the same protocol (F). A subset of NFTs was also stained by thioflavin-S (G). Immunoelectron microscopy revealed the presence of many twisted AT8-positive tau filaments in the basolateral area of the amygdala of

$A\beta_{42}$ -injected P301L mice (H to J). (A) Eight-month-old P301L male analyzed 40 days after injection; (B) 6.5-month-old P301L female analyzed 40 days after injection; [(C) and (D)] Six-month-old P301L female analyzed 18 days after injection; (E) 5.25-month-old P301L male analyzed 21 days after injection; (F) Human 86-year-old female AD patient; (G) Seven-month-old P301L female analyzed 45 days after injection. Bars: 25  $\mu$ m [(A) to (C)], 12.5  $\mu$ m [(D) to (G)], 800  $\mu$ m (H), 100  $\mu$ m (I), 50  $\mu$ m (J).

REPORTS

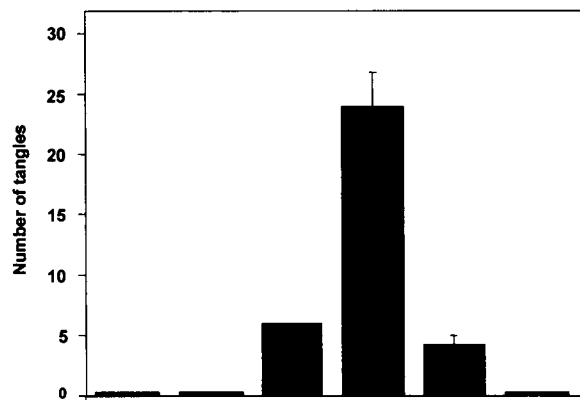
ed ribbons composed mainly of 4R tau. It is therefore possible that the relative amounts of 3R and 4R isoforms contribute to the ultrastructural morphology of the filaments.

Quantitative analyses revealed five times more Gallyas-positive NFTs in the Aβ<sub>42</sub>-injected P301L mice than in Aβ<sub>42-1</sub>- or uninjected P301L mice (Fig. 2, A and B, and Fig. 3). Cross-sectional time-course analyses of NFT formation showed initial NFTs 18 days after Aβ<sub>42</sub> injection, with further increases in numbers (*n* = 58) at least until 60 days after the injection. NFT formation in both hemispheres in the Aβ<sub>42</sub>-injected P301L mice did not vary with gender (females: 23 ± 21; males: 23 ± 4; *n* = 7, *P* = 0.86, Mann-Whitney *U* test). In contrast, Aβ<sub>42-1</sub>-injected P301L males developed few NFTs and P301L females, no NFTs, at 6 to 8.5 months of age. This difference was statistically significant (females: 0; males: 5.8 ± 1.9; *n* = 7, *P* < 0.01, Mann-Whitney *U* test). Importantly, the presence of the tau mutation was necessary for NFT formation be-

cause homozygous transgenic mice expressing human wild-type tau at tau levels similar to or exceeding those of P301L mice (2) failed to develop NFTs in response to Aβ<sub>42</sub> either at 6 or 12 months of age.

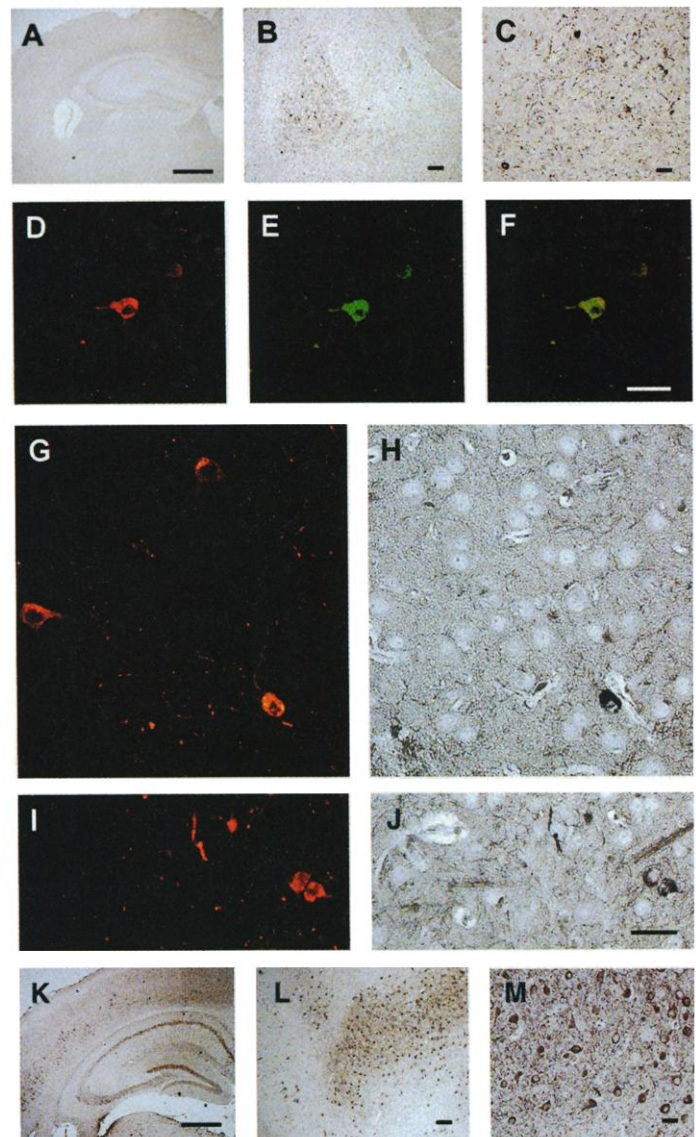
An unexpected finding was the spatial separation of the site of Aβ<sub>42</sub> injection and remote NFT formation in the amygdala, with no significant differences between the ipsilateral and the contralateral amygdala (11.4 ± 10.13 and 9.4 ± 8.0; *n* = 7, *P* = 0.058, Wilcoxon Signed Ranks Test). This finding suggests the possibility that damage to presynaptic terminals or axons of neurons that project to the injection site caused NFT formation in the respective cell bodies. The anatomical separation of amyloid deposition and NFT formation is therefore consistent with Aβ<sub>42</sub>-induced axonal damage and, possibly, impaired axonal transport of tau (15). We confirmed that the affected neuronal population in the amygdala projected to the cortical injection sites by showing retrograde transport of Texas red-conjugated dextran from the in-

jection sites to the amygdala (Fig. 1F). Other mechanisms of somatodendritic accumulation of tau are less likely: First, we excluded a direct exposure to Aβ<sub>42</sub> fibrils of the cell bodies in the amygdala by immunohistochemistry. Second, increases in synthesis of tau protein are unlikely, as indicated by the absence of axonal dilations or spheroids in amygdala neurons. Third, a diffusible toxic factor would hardly explain the failure of neurons adjacent to the injection sites to develop NFTs. Moreover, selective vulnerability of the amygdala for NFT formation is suggested by doubly transgenic mice expressing both mutant APP and P301L tau (16). In human patients with AD, an anatomical separation of amyloid plaques and NFTs is frequently found, with amyloid deposits around synapses and NFTs in the respective cell bodies of projection neurons (17). In addition, the amygdala is among the most vulnerable areas affected early by NFT formation in human patients (18). High vulnerability of the amygdala in our P301L mice is supported by



	wt Aβ <sub>42</sub>	wt Aβ <sub>42-1</sub>	P301L uninj.	P301L Aβ <sub>42</sub>	P301L Aβ <sub>42-1</sub>	wt-tau Aβ <sub>42</sub>
Age (months)	6.3 ± 0.3	6.3 ± 0.3	7	6.4 ± 1.2	7.1 ± 0.7	9.2 ± 2.6
Number of mice	3	3	2	7	7	4

**Fig. 3 (left).** Gallyas-positive NFTs in the amygdala. NFTs were counted on day 22 after injection in Aβ<sub>42</sub><sup>-</sup>, Aβ<sub>42-1</sub><sup>-</sup>, and uninjected P301L transgenic mice, nontransgenic littermate controls, and transgenic mice expressing wild-type human tau (37). The mean age (months ± SD) at the time of analyses is indicated. Gallyas-positive NFTs were counted according to (8) and represent the sum in 20 standardized frontal sections comprising both the ipsilateral and the contralateral amygdala. Mann-Whitney *U* test: *P* = 0.007 (two-tailed exact significance) comparing Aβ<sub>42</sub><sup>-</sup> with Aβ<sub>42-1</sub><sup>-</sup>-injected P301L mice. **Fig. 4 (right).** Abnormal phospho-epitopes of tau induced by Aβ<sub>42</sub> fibrils. The R145d epitope S422 was not phosphorylated in the hippocampus and cortex (A), but was specifically induced by Aβ<sub>42</sub> fibrils in the amygdala [(B); higher magnification: (C)]. Double immunofluorescence staining with R145d (tau phospho-epitope S422) and AT100 (phospho-epitope S212/T214) revealed that R145d-positive neurons in the amygdala were AT100-positive [(D) and (E); merge: (F)]. About half of the R145d-positive neurons (G and I) bore Gallyas-positive NFTs (H and J), and generally these included the neurons that were most intensely stained by R145d. In contrast to R145d and AT100, the AT8 epitope was phosphorylated in many neurons of the hippocampus, cortex (K), and amygdala [(L); higher magnification: (M)]. [(A) to (F), (L) and (M)] Six-month-old P301L male analyzed 18 days after injection; [(G) to (J)] Seven-month-old P301L female analyzed 45 days after injection. Bars: 100 μm [(A), (B), (K), (L)]; 25 μm [(C) and (M)]; 40 μm [(F) and (J)].



the fact that neurons in the amygdala expressed similar levels of the transgene as compared with cortical or hippocampal pyramidal neurons, yet these developed hardly any NFTs (2).

Although our experiments did not formally address the involvement of astrocytes and microglia in NFT formation, activation of these cells alone was not sufficient for NFT formation because A $\beta$ <sub>42</sub> and A $\beta$ <sub>42-1</sub> similarly activated astrocytes and microglial cells, both around the injection sites and in the amygdala (Fig. 1, D and E) (19).

The formation of NFTs in AD is associated with hyperphosphorylation and conformational changes of tau (20–22). To determine whether the A $\beta$ <sub>42</sub>-induced NFT formation in P301L mice was associated with altered phosphorylation and conformation of tau, we used antibodies directed against abnormal phospho-epitopes (R145d, pS<sup>422</sup>, AT100, TG3) (23–25), hyperphosphorylated epitopes (AT8, S199P, AT180, 12E8, AD2, PHF1) (23, 26–31), as well as conformation-dependent antibodies (TG3, MC1) (22, 24), using standard procedures (8, 32).

Whereas several antibodies, including AT8, detected phosphorylated tau throughout the brains of P301L mice independently of the injections, R145d/pS<sup>422</sup> and AT100 directed against phospho-epitopes S422 and S212/T214, respectively, specifically detected NFTs and neurons only in response to A $\beta$ <sub>42</sub> (Fig. 4, A to F). The spatial distribution pattern of these abnormally phosphorylated forms of tau was identical to that observed by Gallyas stainings and occurred, again, predominantly in the amygdala (Fig. 4, A to C). Costaining revealed that neurons stained by R145d/pS<sup>422</sup> were also stained by AT100 (Fig. 4, D to F). Neither R145d nor AT100 immunostained any cells in nontransgenic mice. The specificity of R145d, pS<sup>422</sup>, and AT100 immunoreactivity for A $\beta$ <sub>42</sub>-associated abnormal phosphorylation was exceptional because these antisera revealed few signals in uninjected or A $\beta$ <sub>42-1</sub>-injected P301L tau transgenic mice, and none in transgenic mice expressing wild-type human tau (19). Moreover, all Gallyas-positive NFTs were also stained by R145d, as indicated by sequential immunofluorescence and Gallyas silver impregnation protocols, strongly suggesting that the NFTs in P301L mice contained S422-phosphorylated tau. Semiquantitative analyses revealed that about one-half of the R145d-positive neurons (Fig. 4, G and I) were Gallyas-positive (Fig. 4, H and J), and R145d stained these neurons generally more intensely than cells without NFTs.

Together, the result obtained with immunostaining is consistent with the possibility that phosphorylation of epitopes Ser-212/Thr-214 and Ser-422 is tightly associated with NFT formation. Our data extend previous findings that A $\beta$ <sub>42</sub> induced tau

phosphorylation in vitro and in vivo at the AT8 and 12E8/Ab31 epitopes (33, 34): In our P301L mice, tau was phosphorylated at these epitopes, even in the absence of injected A $\beta$ <sub>42</sub>. Therefore, these epitopes may be necessary but were not sufficient for NFT formation in P301L mice. By using R145d/pS<sup>422</sup> and AT100, we found that A $\beta$ <sub>42</sub> injections were followed by phosphorylation of tau at S212/T214 and S422, suggesting a role of these epitopes in NFT formation.

In summary, our data establish that A $\beta$ <sub>42</sub> fibrils can significantly accelerate NFT formation in P301L mice and provide further support for the hypothesis that  $\beta$ -amyloid can be a causative pathogenic factor. Our data do not exclude the possibility that other factors can also induce NFT formation in brain, in view of the many tauopathies associated with NFT formation in the absence of  $\beta$ -amyloid plaques (3, 35). Our data show that, in transgenic mice, the interaction of  $\beta$ -amyloid with the P301L mutation was required for NFT formation—neither  $\beta$ -amyloid nor the mutation alone was sufficient to generate high numbers of NFTs. Moreover, the mice generated here provide an in vivo assay to determine whether amyloid-lowering therapies such as A $\beta$  vaccination are effective in preventing NFT formation in vivo.

References and Notes

1. J. Lewis et al., *Nature Genet.* **25**, 402 (2000).
2. J. Gotz, F. Chen, R. Barmettler, R. M. Nitsch, *J. Biol. Chem.* **276**, 529 (2001).
3. J. Gotz, *Brain Res. Brain Res. Rev.* **35**, 266 (2001).
4. To generate transgenic mice, we introduced the human pathogenic tau mutation P301L into the cDNA encoding the longest human brain tau isoform by a polymerase chain reaction (PCR)-mediated approach. This isoform contained exons 2 and 3 as well as four microtubule-binding repeats (2<sup>+</sup>3<sup>+</sup>4R, htau40). To discriminate P301L tau transgenic from wild-type tau transgenic mice, we introduced a silent mutation into the P301L construct that destroys a diagnostic Sma I restriction site. The cDNA was conferred with a Kozak consensus sequence and was subcloned into a murine Thy.1.2 genomic expression vector (provided by H. van der Putten, Novartis, Basel). Vector sequences of this construct (named pR5) were removed before microinjection. Transgenic mice were produced by pronuclear injection of B6D2F1  $\times$  B6D2F1 embryos. Founders were identified by PCR analysis of lysates from tail biopsies with two different primer pairs. Founder animals were intercrossed with C57BL/6 mice to establish lines. Transgenic mice were screened with oligonucleotides tau-I (5'-GGAGTTC-GAAGTGAATGGAAG-3') and tau-K (5'-GGTTTTT-GCTGGAATCTGG-3') and yielded an amplification product of 500 base pairs. A restriction digest of the amplification product by Sma I confirmed the presence of the P301L transgene. Of 10 independent transgenic lines, 4 had comparable expression levels as determined by immunoblot analysis. Line pR5-183 was used in the present study.
5. K. B. J. F. a. G. Paxinos, *The Mouse Brain in Stereotaxic Coordinates* (Academic Press, San Diego, 1997).
6. A $\beta$ <sub>42</sub> (Bachem, H-1368, lot 524548) and A $\beta$ <sub>42-1</sub> (Bachem, H-3976, lot 536763) were reconstituted in phosphate-buffered saline (PBS) at a final concentration of 250  $\mu$ M, shaken at 1000 rpm for 84 hours at 37°C in an Eppendorf thermomixer, and analyzed by electron microscopy. Preparations were placed on

carbon-coated 300-mesh grids and stained with 2% phosphotungstic acid. The preparation of the reverse peptide A $\beta$ <sub>42-1</sub> consisted of insoluble aggregates that were not readily detectable by negative contrasting in electron microscopy (Fig. 1B). Micrographs were recorded at an operating voltage of 80 to 100 kV and at nominal magnifications of  $\times$ 40,000 on a Philips model CM12 electron microscope.

7. Mice were anaesthetized with a mixture of 2% Xylazine and 10% Ketamin and stereotaxically injected with 1.5  $\mu$ l of peptide suspension into the CA1 region of the hippocampal formation of the right hemisphere (coordinates: AP -1.9 mm from the bregma, LAT -1.0 mm, DV +1.9 mm), and into the cortex of the left hemisphere (coordinates: AP -1.9 mm from the bregma, LAT +2.0 mm, DV +1.2 mm; includes the trunk region of the somatosensory cortex 1, S1Tr), with a 10- $\mu$ l Hamilton syringe driven by a mini pump (Motorized Stereotaxic Injector, Stoelting), with an injection speed of 0.15  $\mu$ l/min. The needle was kept in the injection site for another 10 min and then slowly withdrawn. Operated animals were monitored daily. None of the mice developed infections or died during the experiment. Injected mice were perfused transcardially with 4% paraformaldehyde in sodium phosphate buffer (pH 7.4) on days 18, 26, 45, and 60, respectively, and processed for immunohistochemistry. To determine axonal uptake, we injected 1.5  $\mu$ l of 12.5 mg/ml Texas red-coupled dextran (molecular weight 70,000, Molecular Probes) in PBS and perfused the mice 5 to 8 days later.
8. Immunohistological stainings were done on 4- $\mu$ m coronal paraffin sections from brain, according to standard procedures. Serial frontal sections were taken, and brain sections from AD patients and healthy humans were included as controls. Some of the sections were pretreated with 5  $\mu$ g/ml proteinase K in tris-buffered saline or PBS at 37°C for 2.5 min for signal enhancement. Sections were stained with thioflavin-S and silver-impregnated by the Gallyas protocol. For Gallyas stainings, every 20th section was analyzed from positions AP -1.5 mm to AP -2.4 mm (from the bregma), whereas every 5th section was analyzed around the injection site (position AP -1.9 mm) from positions AP -1.8 mm to AP -2.0 mm. Gallyas-positive NFTs were counted in 20 standardized frontal sections of total brain from each mouse, and added. Means  $\pm$  SDs were determined for the numbers of mice indicated in Fig. 3. Tau14 (Zymed, South San Francisco, CA; amino acids 83 to 120, 1:2 dilution) and HT7 (Innogenetics, Belgium; amino acids 159 to 163, 1:200 dilution) were used to detect human tau specifically. The following antibodies were used to detect distinct tau phospho-epitopes (in parentheses): AT270 (Innogenetics, 1:500, Thr-181), AT8 (Innogenetics, 1:50, Ser-202/Thr-205), AT100 (Innogenetics, 1:100, Ser-212/Thr-214), 12E8 (P. Seubert, Elan Pharmaceuticals, South San Francisco, CA; 1:100, Ser-262/Ser-356), AT180 and TG3 (P. Davies, 1:100 and 1:20, respectively, Thr-231/Ser-235), PHF1 (P. Davies, 1:50), S199P (A. Delacourte, 1:100, Ser-199), R145d (K. Iqbal, 1:30, Ser-422) and pS<sup>422</sup> (Biosource, 1:50, Ser-422), and AD2 (C. Mourton-Gilles, 1:10,000, Ser-396/Ser-404). MC1 detected the conformational Alz-50 epitope (P. Davies, 1:20). Monoclonal antibody 6E10 (Serotec, 1:500) was used to detect A $\beta$  peptide. Polyclonal antibody to GFAP (Sigma, 1:400) was used to detect activated astrocytes, and Isolectin B4 (Vector Laboratories, 2  $\mu$ g/ml) was used to detect microglia. Secondary antibodies were obtained from Vector Laboratories (Vectastain ABC kits PK-6101 and PK-6102) for peroxidase-diaminobenzidine stainings, and from Molecular Probes (ALEXA-FLUOR™ series) for immunofluorescence.
9. F. Gallyas, *Acta Morphol. Acad. Sci. Hung.* **19**, 1 (1971).
10. H. Braak, E. Braak, I. Grundke-Iqbal, K. Iqbal, *Neurosci. Lett.* **65**, 351 (1986).
11. A. C. McKee, N. W. Kowall, K. S. Kosik, *Ann. Neurol.* **26**, 652 (1989).
12. M. E. Velasco, M. A. Smith, S. L. Siedlak, A. Nunomura, G. Perry, *Brain Res.* **813**, 329 (1998).
13. For transmission electron microscopy, areas contain-

# Activation by IKK $\alpha$ of a Second, Evolutionary Conserved, NF- $\kappa$ B Signaling Pathway

Uwe Senftleben,<sup>1,2</sup> Yixue Cao,<sup>1</sup> Gutian Xiao,<sup>3</sup> Florian R. Greten,<sup>1</sup> Gertraud Krähn,<sup>1,4</sup> Giuseppina Bonizzi,<sup>1</sup> Yi Chen,<sup>1</sup> Yinling Hu,<sup>1</sup> Abraham Fong,<sup>3</sup> Shao-Cong Sun,<sup>3</sup> Michael Karin<sup>1\*</sup>

In mammals, the canonical nuclear factor  $\kappa$ B (NF- $\kappa$ B) signaling pathway activated in response to infections is based on degradation of I $\kappa$ B inhibitors. This pathway depends on the I $\kappa$ B kinase (IKK), which contains two catalytic subunits, IKK $\alpha$  and IKK $\beta$ . IKK $\beta$  is essential for inducible I $\kappa$ B phosphorylation and degradation, whereas IKK $\alpha$  is not. Here we show that IKK $\alpha$  is required for B cell maturation, formation of secondary lymphoid organs, increased expression of certain NF- $\kappa$ B target genes, and processing of the NF- $\kappa$ B2 (p100) precursor. IKK $\alpha$  preferentially phosphorylates NF- $\kappa$ B2, and this activity requires its phosphorylation by upstream kinases, one of which may be NF- $\kappa$ B-inducing kinase (NIK). IKK $\alpha$  is therefore a pivotal component of a second NF- $\kappa$ B activation pathway based on regulated NF- $\kappa$ B2 processing rather than I $\kappa$ B degradation.

Mammals express five NF- $\kappa$ B transcription factors: RelA, RelB, c-Rel, NF- $\kappa$ B1, and NF- $\kappa$ B2 (1). Unlike the Rel proteins, NF- $\kappa$ B1 and NF- $\kappa$ B2 are synthesized as large precursors (p105 and p100, respectively) that require proteolytic processing to produce their respective p50 and p52 NF- $\kappa$ B subunits (1). Mature NF- $\kappa$ B dimers are kept in the cytoplasm through interaction with inhibitory I $\kappa$ B proteins, and the major pathway leading to their activation is based on inducible I $\kappa$ B degradation (1, 2). This canonical pathway, triggered by proinflammatory cytokines, microbes, and viruses, requires activation of the IKK complex (2). Because the NF- $\kappa$ B1 and NF- $\kappa$ B2 precursors contain I $\kappa$ B-like ankyrin repeats in their COOH-termini, they can function as I $\kappa$ Bs (3, 4). Unlike I $\kappa$ B degradation, processing of NF- $\kappa$ B1 is a constitutive process (5, 6). NF- $\kappa$ B2 processing, however, could be a regulated process because it is most active in mature B cell lines (7) and is defective in *aly* mice (8). The *aly* mutation, which maps to the gene encoding NIK, interferes with the development of primary and secondary lymphoid organs (9), as does a complete NIK deficiency (10). Interestingly, NIK induces ubiquitin-dependent processing of NF- $\kappa$ B2 (11) but is not required for induction of NF- $\kappa$ B DNA binding activity (12).

NIK was discovered as an NF- $\kappa$ B-activating kinase (12) and was later shown to phos-

phorylate and activate IKK $\alpha$  (13), one of the two catalytic subunits of the IKK complex (2). The other catalytic subunit, IKK $\beta$ , is 52% identical to IKK $\alpha$  (2), and in vitro both subunits exhibit I $\kappa$ B kinase activity (14). Despite these similarities, IKK $\alpha$  and IKK $\beta$  have distinct functions (2, 5). IKK $\beta$  is essential for proper activation of NF- $\kappa$ B in response to proinflammatory stimuli and for prevention of tumor necrosis factor (TNF- $\alpha$ )-induced apoptosis (15–18), whereas IKK $\alpha$  is dispensable for IKK activation and induction of NF- $\kappa$ B DNA binding activity in most cell types (17, 19). IKK $\alpha$ , but not IKK $\beta$ , is essential for proper skeletal morphogenesis and differentiation of the epidermis (19, 20). However, this function does not depend on IKK activity or NF- $\kappa$ B activation (21). These findings raise the question of whether IKK $\alpha$  has any NF- $\kappa$ B-related functions that are masked by the perinatal lethality of *Ikk $\alpha$ <sup>-/-</sup>* mice. Here, we provide evidence that IKK $\alpha$  kinase activity is required for B cell maturation, formation of secondary lymphoid organs, induction of a subset of NF- $\kappa$ B target genes, and inducible NF- $\kappa$ B2 processing. This function of IKK $\alpha$  is strikingly similar to that of *Drosophila* IKK, which is required for processing of Relish, a NF- $\kappa$ B2-like precursor protein (22, 23). In addition to explaining the function of IKK $\alpha$ , these results shed new light on the mechanisms involved in the evolution of innate and adaptive immunity.

Analysis of bone marrow cells from wild-type, *Ikk $\alpha$ <sup>-/-</sup>*, and *Ikk $\beta$ <sup>-/-</sup>* radiation chimeras (24) revealed complete absence of B cells in *Ikk $\beta$ <sup>-/-</sup>*-derived samples (25). By contrast, B cells were present in *Ikk $\alpha$ <sup>-/-</sup>* reconstituted bone marrow (25). Although these cells expressed normal levels of early B cell markers, a B220<sup>hi</sup>CD24<sup>lo</sup> population, representing circulating mature B cells, was absent (25). No differences in absolute numbers of thymo-

ing the amygdala were excised from 40- $\mu$ m-thick vibratome sections and fixed in 4% paraformaldehyde and 0.1% glutaraldehyde in PBS. After fixation with OsO<sub>4</sub>, tissue samples for routine electron microscopy were embedded in epoxy resin (Epon, Sigma, Bornem, Belgium). For immunogold labeling, ultrathin sections from epoxy resin-embedded tissues on formvar-coated nickel grids were treated with 6% sodium metaperiodate for 10 min and with 5% normal goat serum in PBS for 30 min. This was followed by incubating the sections with monoclonal antibody AT8 in 1% normal goat serum in PBS at a dilution of 1:50 for 2 hours. After washing, 10-nm colloidal gold-tagged secondary antibody in tris-buffered saline (goat anti-mouse; British Biocell, Cardiff, UK) was applied for 1 hour. Then, after washing, sections were stained with lead citrate and uranyl acetate. Control sections were stained following the same procedure, but with omission of the primary antibody. AT8 appeared to label frequently "ends" of filaments because filaments sectioned at the surfaces of the epoxy-embedded preparations were more easily accessible to the antibodies than were deeper layers.

14. M. G. Spillantini et al., *Am. J. Pathol.* **153**, 1359 (1998).
15. S. Varadarajan, S. Yatin, M. Aksanova, D. A. Butterfield, *J. Struct. Biol.* **130**, 184 (2000).
16. J. Lewis et al., *Science* **293**, 1487 (2001).
17. D. L. Price, S. S. Sisodia, *Annu. Rev. Med.* **45**, 435 (1994).
18. S. E. Arnold, B. T. Hyman, J. Flory, A. R. Damasio, G. W. Van Hoesen, *Cereb. Cortex* **1**, 103 (1991).
19. J. Götz, F. Chen, J. van Dorpe, R. M. Nitsch, data not shown.
20. I. Grundke-Iqbal et al., *Proc. Natl. Acad. Sci. U.S.A.* **83**, 4913 (1986).
21. H. Braak, E. Braak, *Neurobiol. Aging* **16**, 271 (1995).
22. G. A. Jicha, R. Bowser, I. G. Kazam, P. Davies, *J. Neurosci. Res.* **48**, 128 (1997).
23. M. Goedert et al., *Biochem. J.* **301**, 871 (1994).
24. D. W. Dickson et al., *Neurobiol. Aging* **16**, 285 (1995).
25. T. Tanaka, J. Zhong, K. Iqbal, E. Trenkner, I. Grundke-Iqbal, *FEBS Lett.* **426**, 248 (1998).
26. S. G. Greenberg, P. Davies, J. D. Schein, L. I. Binder, *J. Biol. Chem.* **267**, 564 (1992).
27. M. Goedert, R. Jakes, E. Vanmechelen, *Neurosci. Lett.* **189**, 167 (1995).
28. P. Seubert et al., *J. Biol. Chem.* **270**, 18917 (1995).
29. V. Buee-Scherrer et al., *Brain Res. Mol. Brain Res.* **39**, 79 (1996).
30. A. Delacourte, N. Sergeant, A. Wattez, D. Gauvreau, Y. Robitaille, *Ann. Neurol.* **43**, 193 (1998).
31. N. Sergeant, A. Wattez, A. Delacourte, *J. Neurochem.* **72**, 1243 (1999).
32. J. Gotz, A. Probst, E. Ehler, B. Hemmings, W. Kues, *Proc. Natl. Acad. Sci. U.S.A.* **95**, 12370 (1998).
33. J. Busciglio, A. Lorenzo, J. Yeh, B. A. Yankner, *Neuron* **14**, 879 (1995).
34. C. Geula et al., *Nature Med.* **4**, 827 (1998).
35. L. Buee, T. Bussiere, V. Buee-Scherrer, A. Delacourte, P. R. Hof, *Brain Res. Brain Res. Rev.* **33**, 95 (2000).
36. K. K. Hsiao et al., *Neuron* **15**, 1203 (1995).
37. A. Probst et al., *Acta Neuropathol. (Berlin)* **99**, 469 (2000).
38. We thank E. Moritz, D. Schuppli, B. Knecht, and H.-P. Gautschi for technical assistance and J. Opoku for animal care. We also thank P. Davies (Bronx, NY) for antibodies PHF1, TG3, and MC1; P. Seubert (Elan Pharmaceuticals, South San Francisco) for antibody 12E8; A. Delacourte for antiserum S199P; K. Iqbal for antibody R145d; and C. Mourton-Gilles (Lille, France) for antibody AD2. We thank T. Baechli for providing the electron microscopy facility and members of his laboratory for assistance, and M. Glatzel for suggesting the use of Texas red-coupled dextran. Supported by the University of Zürich and, in part, by grants from Evotec NeuroSciences, Bayer Pharma AG (BARN; Bayer Alzheimer's Disease Research Network), the Swiss National Foundation (SNF), and the National Center for Competence in Research (NCCR) "Neuronal Plasticity and Repair."

30 April 2001; accepted 11 July 2001

<sup>1</sup>Laboratory of Gene Regulation and Signal Transduction, Department of Pharmacology, University of California, San Diego, 9500 Gilman Drive, La Jolla, CA 92093, USA. <sup>2</sup>Clinic for Anesthesiology, University of Ulm, Steinhövelstrasse 9, 89075 Ulm, Germany. <sup>3</sup>Department of Microbiology and Immunology, Pennsylvania State University College of Medicine, Hershey, PA 17033, USA. <sup>4</sup>Department of Dermatology, University of Ulm, Oberer Eselsberg 40, 89081 Ulm, Germany.

\*To whom correspondence should be addressed.